Bimetallic Nanostructured Catalysts Prepared by Laser Electrodispersion: Structure and Activity in Redox Reactions

A. A. Bryzhin,[a] E. V. Golubina,[a] K. I. Maslakov,[a] E. S. Lokteva,[a] I. G. Tarkhanova,[a] S. A. Gurevich,[b] D. A. Yavsin,[b] and T. N. Rostovshchikova*[a]

One-stage size-selective method of laser electrodispersion (LED) was used to produce nanostructured NiPd, NiMo and NiW coatings on the surface of alumina, HOPG and Sibunit for the catalytic application. The deposition of nanoparticles produced by LED of bimetallic targets from alloyed or pressed metal powders provides the uniform distribution of both metals on the outer support surface; the metal ratio is similar to that in the original target. The catalytic behaviour of produced "core-shell" catalysts in comparison with monometallic analogues was tested in two model reactions: the CO oxidation with oxygen on NiPd catalysts supported on alumina and Sibunit; and thiophene oxidation with hydrogen peroxide on NiMo and NiW alumina supported catalysts. Novel LED bimetallic catalysts with extremely low metal content (0.005 %) were superior in terms of activity and stability to monometallic ones and the catalysts obtained by "wet" chemistry methods. Improved catalytic properties of bimetallic LED catalysts are related to the high density of single nanoparticles and the formation of active metal-oxide interfaces on the support surface.

Introduction

Bimetallic catalysts are widely applied in industry because of their enhanced catalytic properties compared to monometallic catalysts and reduced content of noble metals.[1–3] However, the chemical synthesis of bimetallic catalyst is typically a multistage process, which is far from easy to realize. Achieving monodispersed bimetallic particles of uniform shape and composition still remains a challenge.[4] Physical methods of deposition of nanostructured catalysts on the base of laser ablation allow to overcome these difficulties and synthesise bimetallic catalysts in one stage under environmentally friendly and reproducible conditions.[5–8]

Among ablation techniques the laser electrodispersion (LED) stands out for its ability to produce monodispersed metal drops in the laser plasma torch. Their deposition on the support surface makes it possible to produce "core-shell" size-selected catalysts in one stage without auxiliary chemical reagents, reduction agents and stabilizers, with these catalysts being unusually stable against aggregation and sintering.[9] The uniform distribution of finely dispersed amorphous nanoparticles only on the outer support surface provides high activity of LED catalysts at extremely low metal loadings (up to 10^{-3} wt.%). LED catalysts strongly differ in structure, adsorption and catalytic properties from supported catalysts synthesized by "wet" chemical methods.[10–12]

The scheme of the LED process is shown in Figure 1. A high power pulse laser is used to melt the metal target surface. During each pulse the surface layer of the target melts, evaporates, and the optical breakdown of metal vapour leads to the formation of plasma (laser torch). Under the influence of the plasma pressure metal microdrops escape the melted surface of the target coming into laser torch plasma. These microdrops are charged in the plasma up to the capillary instability threshold, at which their cascade fission starts. Smaller and smaller molten metal particles are generated during fission, and finally divided drops of equal size fall on the surface of the support.

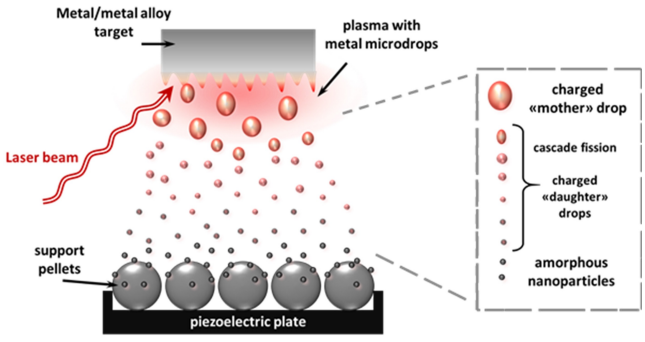

Figure 1. Scheme of nanoparticle deposition by LED.

[a] A. A. Bryzhin, E. V. Golubina, K. I. Maslakov, E. S. Lokteva, I. G. Tarkhanova, Prof. T. N. Rostovshchikova
Department of Chemistry
Lomonosov Moscow State University
Leninskie Gory, 1/3
119991, Moscow (Russia)
E-mail: rtn@kinet.chem.msu.ru
[b] S. A. Gurevich, D. A. Yavsin
Ioffe Physical-Technical Institute of RAS
Politekhnicheskaya, 26
194021, Saint Petersburg (Russia)

Supporting information for this article is available on the WWW under https://doi.org/10.1002/cctc.202000501

The main advantage of this method is that the particle size of metal catalysts deposed by LED is independent of both the support type and the surface coverage degree.[9,13] The fast cooling of monodispersed nanodrops preliminarily produced in the laser plasma torch during their deposition on the support surface preserves their size, spherical shape and amorphous structure. Monometallic LED catalysts comprising Pd, Pt, Ni, Cu supported on carbon and oxide supports were widely studied in several classes of catalytic reactions,[9–13] and very promising results were achieved in environmentally important reactions of hydrodechlorination of chlorinated organic molecules. However bimetallic LED catalysts were synthesized only recently.[14,15]

The Pd–Ni active component is one of the most interesting for catalytic systems. Recently the possibility to produce a bimetallic coating on the alumina surface using the NiPd alloy target for LED deposition has been shown.[14] These bimetallic catalysts with the total metal loading of 0.005 wt.% demonstrated higher activity and stability in chlorobenzene hydrodechlorination than their monometallic Pd counterparts. Monometallic Ni LED catalysts showed low activity and were rapidly chlorinated in this reaction.

Compacted mixture of metal powders can be also used as a LED target for deposition of bimetallic coatings. NiMo and NiW nanoparticles supported by LED on γ-Al_2O_3 showed high efficiency in oxidation of sulfur-containing substrates with hydrogen peroxide.[15] This process is of practical importance for the development of new oxidative oil desulfurization methods as an alternative to the traditional hydrotreating. Oxidative catalysts are typically pure and complex oxides or metallates of Mo, W or other V–VI group metals.[16] Ni-containing systems are at the same time adsorbents and catalysts for two processes – hydrogenation and oxidation.[17] These polyfunctional catalysts are of special interest because they can be used both in hydrotreating and oxidative desulfurization.[18] There are two reasons for the choice of thiophene as a model substrate for oxidative desulfurization. Firstly, thiophene is the most resistant to oxidation among thiophene derivatives contained in fuels.[18] Secondly, we earlier observed the formation of sulfuric acid during oxidation of thiophene on tungsten-containing catalysts.[19] As a result, the corrosion medium is formed, which may decompose the catalyst.[20] Therefore, the selected process allows testing both the activity and stability of catalysts.

In this work we widen the scope of the application of LED method to the synthesis of various types of bimetallic catalysts, including Ni-containing ones, for the practically important processes of environmental catalysis. For this purpose, bimetallic NiPd nanoparticles were deposited on different types of supports (alumina, HOPG, and Sibunit) by LED of the alloy target, while bimetallic NiMo and NiW catalysts were deposited on alumina support by LED of compacted mixture of metal powders. Their monometallic counterparts were produced by the same technique for comparison. NiPd catalysts were tested in the model reaction of CO oxidation with oxygen, while NiMo/W systems – in thiophene oxidation with hydrogen peroxide. The main feature of these catalysts is the "core-shell" distribution of single nanoparticles on support surface, which makes the active component of the catalyst readily available to reactants even at low metal loading (10^{-3} wt.%).

Results and Discussion

Catalyst structure

The estimation and comparison of metal loadings in LED systems produced on flat and granulated supports is a challenging task; the detailed description of metal loading calculation for flat (carbon-coated Cu TEM-grids (C-grids) and HOPG) and granulated supports (alumina and Sibunit) is presented in Tables S1 and S2 in Supporting Materials (SM). Further in this article the metal loadings on model flat supports will be presented as the degree of surface coverage with nanoparticles in the form of the number of layers of metal nanoparticles on a carrier surface (NPL); for granulated supports – in wt.%; the comparison of metal loadings in flat and granulated catalysts can be made on the base of Tables S1 and S2 in SM.

NiPd catalysts

Results of the TEM and XPS study of monometallic Ni, Pd and bimetallic NiPd LED coatings are detailed in.[10,14,21] According to these works Pd and Ni metal nanoparticles in monometallic samples were about 2 nm in size independently on the support type and metal loading. This is confirmed by the example of Pd nanoparticle images on C-grid shown in Figure 1, SM. The particle size distribution only slightly changed for different surface coverage from 1.0 to 0.1 NPL. The uniform distribution of size-selected NiPd particles of about 1 nm in size was found in bimetallic catalysts deposited by LED from the $Ni_{77}Pd_{23}$ alloy.[14] According to STEM/EDS data for NiPd/Al_2O_3 (Figure S2, SM), both metals were located at the same areas on the catalyst surface and in all analysed areas nickel prevails over palladium about 3 times. These data may be considered as an evidence for the formation of bimetallic particles, or at least both metals are situated in close vicinity.

The electronic state of Ni and Pd on the surface of mono- and bimetallic LED catalysts supported on alumina granules was thoroughly studied by XPS. In XPS spectra of monometallic catalysts components related to metallic (Pd^0, Ni^0) and oxidized (Pd^{2+}, Ni^{2+}) states were observed.[10,21,22] The typical spectra of Pd/Al_2O_3 granule, initial and after reduction with H_2 at 150 °C, are shown in Figure S3, SM. The presence of distinct signals at such a low metal content (0.005 wt.%) indicates the "crust-like" distribution of metal on the outer surface of the support granule; the signals disappeared after crushing of the catalyst's granules.

Results of the decomposition of earlier published[10,14] XPS spectra for mono- and bimetallic samples are summarized in Table S3, SM.

The values of E_b for metallic states are close to known data for Ni^0[23] and Pd^0.[24] But peaks of oxidized states were observed

at binding energies at 856.0 eV for Ni2p and 338.0 eV for Pd3d that are higher than the values of 854.5 eV for NiO[25] and 336.7 eV for PdO.[24] Such shift can be explained by metal-support interaction (MSI) which may even lead to the formation of nickel aluminate[14] or other mixed oxides[26] e.g. NiO_xPd in bimetallic catalyst.

XPS experiments on in-situ metal reduction have shown that the reducibility of oxidized forms of Ni and Pd is different in bimetallic and monometallic coatings (Table S3, SM); the reduction proceeds much easily in monometallic LED systems. Under hydrogen treatment NiO in Ni/Al_2O_3 catalyst started to reduce at 300 °C. But Ni^{2+} species in $NiPd/Al_2O_3$ were not reducible with H_2 even at 450 °C. The oxidized Pd species on the surface of Pd/Al_2O_3 can be heavily reduced to Pd^0 at 150 °C, but only 32% of Pd in bimetallic $NiPd/Al_2O_3$ transforms to Pd^0 at this temperature. The observed difference in reducibility of metals in mono- and bimetallic catalysts can be caused by smaller particle size and stronger metal-oxide interactions in NiPd system.

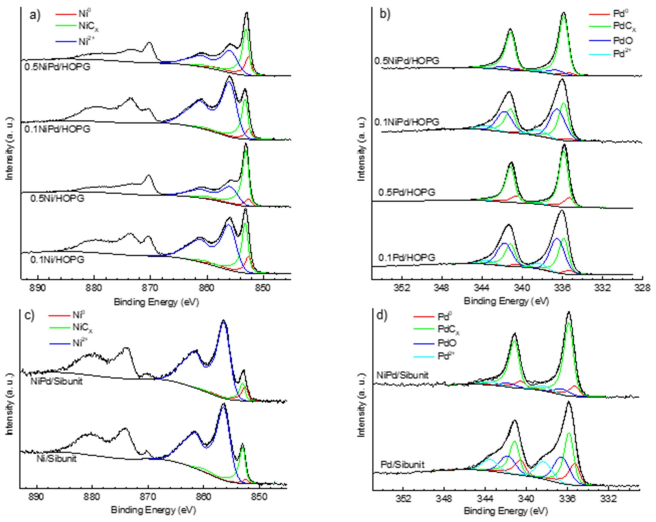

Figure 2. Ni2p (a, c) and Pd3d (b, d) XPS spectra of NiPd, Ni and Pd catalysts with different metal loading: 0.1 and 0.5 NPL on HOPG (a, b); 0.005% on Sibunit (c, d).

It is reasonable to assume that the MSI may be diminished by replacing alumina with a more inert carbon support. To check this assumption two carbon materials – HOPG and Sibunit were used for metal deposition in this work. The former is flat and conducting, and therefore more suitable for model experiments, while the granulated Sibunit is commonly used as industrial adsorbent and catalyst carrier.[27]

Typical XPS spectra of mono- and bimetallic Ni,Pd systems supported by LED on HOPG and Sibunit are presented in Figure 2. $Ni2p_{3/2}$ spectra were fitted with three components (Table 1). The narrow component at the binding energy of 852.6 eV corresponds to metallic Ni,[23,28] while the component centred at 853.1 eV can be assigned to Ni with interstitially dissolved carbon or to surface carbide NiC_x.[28,29] Larger area of this component compared to the Ni^0 component testifies the significant MSI in both Ni-containing samples.

The broad component at the binding energy of about 856 eV with the intensive shake-up satellite is attributed to oxidized Ni^{2+} species. As in the case of alumina supported particles, this binding energy is significantly higher than that for NiO.[25] It cannot be assigned to $Ni(OH)_2$,[30] because the separation distance between the main peak and the satellite (5.1 eV) is lower than that for $Ni(OH)_2$ (about 6 eV) .[30] More probably this component can be attributed to mixed oxides, and also to Ni^{2+} salts,[26] for example, or NiC_xO_Y species resulting from Ni interaction with O-containing functional groups on the Sibunit surface. Two types of Ni species bonding with the surface of the other carbon support – nanodiamond – through oxygen-containing functional groups and directly with the carbon surface were earlier observed in.[31]

The percentage of oxidized species increases with decreasing surface coverage of a support by Ni particles. The same trend was earlier observed for Ni/Al_2O_3 catalysts produced by LED.[22] It was well-established that the particle size in LED coatings is independent on the metal loading or surface density of particles.[9] Therefore, we can propose that the interaction with oxygen-containing surface groups is responsible for the fact that nickel oxidation is higher for isolated particles than for islands of particles in denser layers.

In the same way the $Pd3d_{5/2}$ binding energy for all the samples supported on HOPG and Sibunit is about 0.7 eV higher than that for metallic Pd (335.2 eV[24]) (Figure 2, c, d) probably

Table 1. Percentage of components in $Ni2p_{3/2}$ and $Pd3d_{5/2}$ XPS spectra of NiPd samples supported by LED on HOPG and Sibunit and their attribution to different species.

Sample	Metal loading NPL, (HOPG) or wt.% (Sibunit)	Ni Ni^0 (852.6)[a]	NiC_x (853.1–853.2)	Ni^{2+} (855.9–856.1)	Pd Pd^0 (335.3)	PdC_x (335.9)	PdO (336.5–336.6)	Pd^{2+} (338.2–338.3)
Ni/HOPG	0.1	9	25	66	–	–	–	–
Ni/HOPG	0.5	7	48	45	–	–	–	–
Pd/HOPG	0.1	–	–	–	5	39	48	8
Pd/HOPG	0.5	–	–	–	17	81	–	2
NiPd/HOPG	0.1	6	19	75	2	42	46	10
NiPd/HOPG	0.5	16	34	50	4	84	9	3
Ni/Sibunit	0.005	2	16	82	–	–	–	–
Pd/Sibunit	0.005	–	–	–	19	37	26	18
NiPd/Sibunit	0.005	6	7	87	12	73	8	7

[a] Binding energies of components (eV) are presented in brackets.

because of the palladium interaction with carbon support. Such shift was earlier attributed to the formation of PdC_X species.[32–34] Therefore, to fit $Pd3d_{5/2}$ XPS spectra we also used two narrow components with a binding energy that differs by 0.6 eV and attributed to metallic Pd and PdC_X. Two additional broader components at 336.6 and 338.3 eV may be assigned to PdO,[24] and other Pd^{2+} species, probably, in mixed NiO_xPd oxides or in products of the Pd interaction with oxygen-containing groups on the carbon surface, as it was discussed above for Ni. For example, the same value of $Pd3d_{5/2}$ binding energy (338.3 eV) was found for palladium acetate. The fitting results (Table 1) demonstrate that at high Pd loading the fraction of oxidized Pd species on HOPG is low, while the major part of Pd exists as PdC_X.

The presence of MeC_X species in carbon-supported samples is also confirmed by their C1s spectra (Figure S4, Table S4, SM). The shoulder in these spectra on the low energy side of the main line attributed to sp^2-carbon indicates the presence of MSI. This shoulder is the most pronounced in the spectra of samples with high Ni loading. The fitting of the C1s spectra of the HOPG-supported samples revealed the significant contribution of the component at binding energy of 283.8 eV, that can be attributed both to NiC_X[28,29] and PdC_x[33] species. The contribution from MeC_X species to the Pd3d, Ni2p and C1s spectra is lower for Sibunit-supported samples than for HOPG-supported ones due to the higher fraction of surface functional groups on the Sibunit.[27]

Summarizing, we can conclude, that independently on the type of a support Ni and Pd in LED bimetallic systems are situated in close vicinity, may be in the composition of the same particles, as it is evident from EDS data. According to EDS and XPS studies (Table 2), the Ni/Pd atomic ratio in the samples produced by LED of NiPd alloy target on the surface of alumina or carbon supports (3–3.5) is close to this value in the initial alloy (about 3.35, or 77:23).

Surprisingly Ni and Pd in LED catalysts strongly interact not only with alumina, but also with carbon support. Probably carbide-like species are formed on the surface of nanoparticles during LED deposition of metals. Oxidized metal species also exist on the surface, especially in the samples with low metal coverage. For all HOPG samples the fraction of reduced metal forms is similar in mono- and bimetallic counterparts. In contrast, palladium is more reduced in bimetallic NiPd catalyst on the Sibunit support than in monometallic one, while the amount of reduced nickel does not change. From the comparison of XPS spectra before and after *in-situ* reduction with H_2 (see e.g. Figure S3, SM) it is seen that Me^{2+} in bimetallic samples is much difficult to reduce than in monometallic samples.

Table 2. Surface concentration of elements (at.%, XPS) in Ni, Pd and NiPd catalysts on Sibunit with 0.005 % metal loading.

Catalyst	Ni	Pd	O	C
Pd/Sibunit	–	3.8	5.6	90.6
NiPd/Sibunit	5.3	1.5	18.5	74.7
Ni/Sibunit	9.1	–	26.1	64.8

Mo/W catalysts

Typical SEM image and EDX spectra of monometallic sample (Mo/Al_2O_3) are shown in Figure S5 (SM), metal mapping indicates that Mo is uniformly distributed over the support surface. On the other hand, TEM images of all monometallic catalysts show the absence of high contrast particles that can be attributed to nickel, molybdenum or tungsten in the metallic state. This may be related to oxidized state of metals on the surface of monometallic samples, which are difficult to distinguish on the alumina surface. The presence of particles of different interplanar distances some of which cannot be attributed to alumina phase indirectly confirms this idea. For example, domains with interplanar distance of 0.21 nm that corresponds to NiO (200) were observed in the TEM images of Ni/Al_2O_3 (SM, Figure S6a). The presence of heavy metals is clearly seen in HAADF-STEM images as bright fields contrasted with grey alumina areas (SM, Figure S6b–d).

In contrast to monometallic samples, dark particles 4–7 nm in size were observed in the TEM images of bimetallic NiMo- and NiW/Al_2O_3 samples.[15] Stronger contrast of these particles compared to alumina evidences that they may contain the fraction of non-oxidized metals (Ni, Mo, and W). According to TEM- and STEM-EDS data (Figure S7 and S8, SM), both metals in bimetallic samples are uniformly distributed on the support, regardless of its type (C-grid or alumina surface).

The results of the XPS study of alumina-supported bimetallic NMo and NiW catalysts are shown in SM (Figure S9) and Table 3 in comparison with their monometallic counterparts. As can be seen from Table 3 the atomic ratio of Ni:Mo and Ni:W on the surface of bimetallic catalysts is close to 1, that corresponds to this value (50:50) in the initial mixture.

Fitting of Mo3d and W4f spectra in accordance with[23,30,35] revealed the contribution from several species (Me^0, Me^{4+}, and Me^{6+}), but the percentages of these states are different in mono- and bimetallic samples. According to the fitting results (Table 3), only oxidized metal species (Mo^{4+}, Mo^{6+}, W^{4+}, and W^{6+}) are observed in the monometallic Mo/Al_2O_3 and W/Al_2O_3 catalysts. In contrast, the XPS spectra of bimetallic catalysts revealed the presence not only of oxidized metal species but also Me^0, which confirms the assumption previously made on the base of TEM data. This contribution is especially high in the case of NiW. Indeed, the content of Mo^0 in bimetallic NiMo catalyst is 7 at.% (Table 3), whereas in bimetallic NiW the W^0 percentage is as high as 28 at.%. The percentage of Ni^0 species also increases in bimetallic catalysts compared to monometallic Ni/Al_2O_3 with the similar Ni content. Such high fraction of metallic Ni was observed only for the Ni/Al_2O_3 with ten times higher nickel content (0.05 wt.%) than in its bimetallic counterpart. Therefore, the distinctive characteristic of bimetallic catalysts is the presence of zero-valent metals and different oxidized states of Ni, Mo and W. The appearance of the reduced metal forms in the bimetallic samples may be connected with the intermetallic interaction[36] that can hinder the oxidation of both metals in the oxygen-containing environment. The formation of intermetallic compounds becomes highly probable at extremely high temperatures under laser ablation. The

Table 3. Percentage of $Ni2p_{3/2}$, $Mo3d_{5/2}$, and $W4f_{7/2}$ components in XPS spectra of Ni, Mo and W catalysts supported on alumina and their attribution to different species. The data for bimetallic samples are reproduced from.[15]

Sample	Metal loading, [wt.%] (XPS metal ratio)	Ni		Mo			W		
		Ni^0 (852.6)[a]	Ni^{2+} (855.9)	Mo^0 (227.9)	Mo^{4+} (230.8)	Mo^{6+} (232.4)	W^0 (31.1)	W^{4+} (33.6)	W^{6+} (35.5)
Ni/Al_2O_3	0.05 (Ni/Al = 3.4)	37	67	–	–	–	–	–	–
Ni/Al_2O_3	0.005 (Ni/Al = 0.35)	1	99	–	–	–	–	–	
Mo/Al_2O_3	0.005 (Mo/Al = 0.11)	–	–	0	58	42	–	–	–
W/Al_2O_3	0.005 (W/Al = 0.10)	–	–	–	–	–	0	23	77
$NiMo/Al_2O_3$	0.004 (Ni/Al = 0.28, Mo/Al = 0.31)	19	81	7	35	58	–	–	–
NiW/Al_2O_3	0.007 (Ni/Al = 0.58, W/Al = 0.67)	28	72	–	–	–	28	12	60

[a] Binding energies of components (eV) are presented in brackets.

simultaneous presence of metals and their oxides and the appearance of the metal-oxide interfaces can enhance the catalytic performance.[37] The difference in the electronic state of metals in mono- and bimetallic catalysts determines the features of their catalytic behaviour.

Catalytic properties

CO oxidation with oxygen on mono- and bimetallic NiPd catalysts

Palladium catalysts supported on alumina by common methods usually oxidize CO at relatively high temperature, higher than 150 °C.[38] The light-off temperature significantly depends on the CO/O_2 ratio. Due to the strong CO adsorption on active Pd sites the CO oxidation proceeds at even higher temperature when the stoichiometric ratio of reagents is used instead of oxygen-reach mixture.[39] In this case the light-off temperature on the Pd catalysts synthesized by standard chemical methods shifts to about 200 °C. For example, at the stoichiometric reaction conditions the temperature of 10% CO conversion (T_{10}) on the 0.6%Pd/Al_2O_3 catalyst prepared by deposition-precipitation was in the range of 175–192 °C depending on the catalyst pre-treatment and Pd particle size.[40] Ni/Al_2O_3 catalysts prepared by impregnation were inactive in CO oxidation under these conditions.[41]

Stoichiometric CO/O_2 mixture (2 vol.% CO, 1 vol.% O_2, He balance) was used for testing mono- and bimetallic Ni and Pd LED catalysts with 0.005 wt% metal loading. Figure 3 shows the temperature dependence of CO conversion on $NiPd/Al_2O_3$ catalyst. The values of T_{10} for mono- and bimetallic catalysts are presented in the insert in Figure 3. The comparison of these data demonstrates that not only Pd but also Ni nanoparticles deposited on the alumina support by LED in extremely low amount (0.005 wt.%) show the good activity in CO oxidation. Moreover, T_{10} for Ni catalyst (252 °C) is very close to that for Pd and NiPd ones (Figure 3, insert). Such high efficiency of Ni catalysts in CO oxidation at relatively low temperature is very unusual, and not typical for catalysts prepared by "wet" methods (e.g. by impregnation) and containing only NiO species at such a low Ni content.[22,41] The improved reducibility of Ni in monometallic LED catalysts compared to the commonly

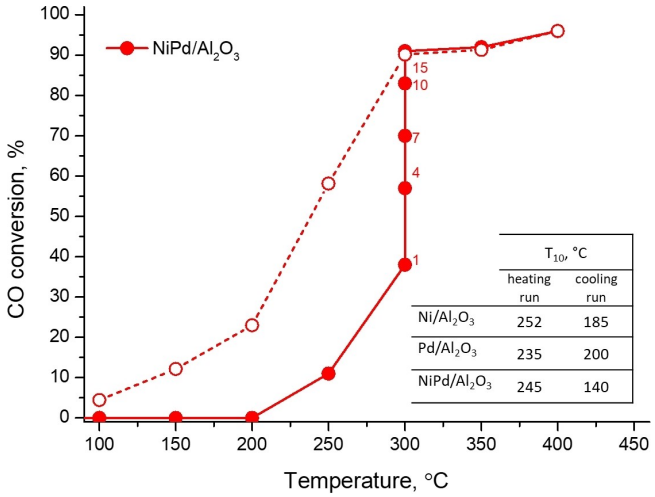

Figure 3. Temperature dependences of CO conversion on 0.005 wt.% $NiPd/Al_2O_3$ catalyst (filled symbols represent heating run while empty symbols – cooling run; pulse number is shown near data points on the isothermal segment of conversion curve). T_{10} temperatures for monometallic Ni and Pd catalysts with 0.005 wt.% metal content reproduced from[10,21] are presented in the insert.

used systems[42] provides simultaneous presence of Ni^0 and Ni^{2+} which can improve the adsorption and catalytic properties of LED catalysts.[12] The theoretical and experimental studies have shown that the CO molecule is more easily activated at the metal-oxide interface due to electron transfer from metal to oxide.[43]

It's worth noting that at 300 °C the CO conversion on the bimetallic $NiPd/Al_2O_3$ catalyst isothermally increased from 40 to 90% with each subsequent pulse of the reaction mixture. This increase was not observed neither at higher nor at lower temperatures (SM, Figure S10). Monometallic catalysts on alumina didn't show this effect. The isothermal increase of conversion may be attributed to the reduction of oxidized metal species under the action of CO.[10] The different reducibility of the active components in mono- and bimetallic catalysts may be the reason of their different catalytic performance. According to the data of Table S3 (SM), the reduction of oxidized Ni and Pd forms proceeds much easily in monometallic LED samples compared to bimetallic ones. Therefore, by the time the reaction begins,

active sites in monometallic catalysts have already been substantially reduced.

Higher CO conversion values on the $NiPd/Al_2O_3$ catalyst were observed at each temperature point in the cooling run than in the heating one (Figure 3). As a result, the T_{10} temperature decreased up to 140 °C in the cooling run. This temperature is lower than those for the monometallic Ni/Al_2O_3 and even for Pd/Al_2O_3 LED catalysts with the same metal loadings, as well as for conventional Pd/Al_2O_3 catalysts with three orders of magnitude higher palladium loading.[40]

The higher light-off temperatures were observed for catalysts on Sibunit support (Figure 4). The Ni/Sibunit catalysts showed the lowest activity: T_{10} was 350 °C, and at 450 °C the CO conversion was only 30%. Palladium containing catalysts (Pd/Sibunit and NiPd/Sibunit) demonstrated higher activity and provided complete CO conversion at 450 °C. As in the case of bimetallic $NiPd/Al_2O_3$, the CO conversion on NiPd/Sibunit isothermally increased at 400 °C. But in contrast to alumina supported catalysts this phenomenon is characteristic also for monometallic Pd/Sibunit sample at lower temperature of 350 °C (SM, Figure S11). The distinction in temperatures of isothermal growth of the conversion for Pd and NiPd/Sibunit samples can be attributed to different electronic states of metals and different nature of the processes leading to this improvement. According to the XPS results, about 40% of Pd in the Pd/Sibunit catalyst is oxidized (PdO and other type of Pd^{2+} species). These oxidized species should be probably reduced at 350 °C (Table S3, SM). By this means, the reduction of Pd^{2+} as well as the transformation of carbide form of Pd may take place in monometallic catalyst.

However, NiPd/Sibunit comprises very low fraction of oxidized metal, while the predominant form of Pd in this sample is PdC_x. Therefore, in this case the isothermal increase of CO conversion can be hardly connected with the additional Pd reduction, the transformation of carbide form into active species should be more important. The role of PdCx and PdO forms in the CO oxidation was earlier discussed for the Pd/CeO_2 catalyst.[44]

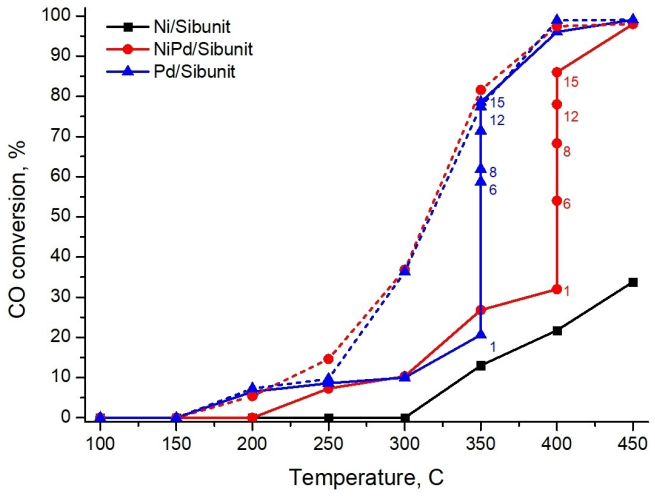

Figure 4. Temperature dependences of CO conversion on Sibunit-supported Ni, Pd, and NiPd catalysts with 0.005 wt.% metal content (pulse number is shown near data points of the isothermal segment of conversion curve).

It should be noted that the reduction of Ni^{2+} in the presence of Pd is usually believed to be a reason for the improvement of catalytic efficiency of common bimetallic NiPd catalysts prepared by "wet" methods. Pd is known to decrease the reduction temperature of the second metal in the bimetallic system via hydrogen spillover from Pd to oxidized species.[45] However, this is not the case for LED prepared systems. Indeed, the comparison of XPS data presented in Table 1 for Ni/Sibunit and NiPd/Sibunit demonstrates the similar content of Ni^{2+} species (82% and 87%) but their catalytic performance is different.

All three Sibunit-supported catalysts show catalytic action at about 100 °C higher temperatures than their counterparts supported on alumina. This probably results from the stronger interaction of Pd with carbon than with alumina, which is confirmed by the high percentage of PdC_x species detected by XPS.

As discussed above, the efficiency of CO oxidation strongly depends on CO/O_2 ratio in the reaction mixture. The comparison of our results with literature data is only possible for the catalysts tested under the same conditions. Earlier bimetallic $CuPd/Al_2O_3$ and $NiAu/Al_2O_3$, catalysts synthesized by conventional impregnation and ion exchange methods were tested in CO oxidation using the same stoichiometric CO/O_2 mixture.[40,41]

Table 4 shows the comparison of TOF values for LED catalysts synthesized in our work with the literature data. TOF values were calculated at 250 °C in accordance with equation based on Basset-Habshood kinetics.[47] Detailed description of the calculation based on CO conversion vs. temperature dependencies obtained in pulse mode is presented in S3, SM. Only the amount of Pd in the NiPd/Sibunit catalyst was taken into account in the calculation, since Ni was not active at this temperature. It's clearly seen that LED catalysts show orders of magnitude higher activity than that of conventional catalysts. Such a high activity of LED catalysts results from fine dispersion of metal particles and their distribution over the external surface of support pellets.[48] Comparison of the LED catalysts supported on both Sibunit and Al_2O_3 shows that the activity of bimetallic catalysts is higher than that of monometallic samples. This may result from the interaction of metallic and oxidized Pd and Ni species with each other and with the support. According to,[49] the CO oxidation occurs in two stages: the acceptor stage when oxygen accepts electrons from the nanoparticle and the

Table 4. TOF values for CO oxidation on LED and conventional catalysts at 250 °C.

Catalyst	Metal loading [wt.%]	TOF [s^{-1}]	Ref.
NiPd/Sibunit	0.005	16	This work
Pd/Sibunit	0.005	4	This work
Ni/Sibunit	0.005	0	This work
$NiPd/Al_2O_3$	0.005	26	This work
Pd/Al_2O_3	0.005	7	[21]
Ni/Al_2O_3	0.005	4	[12]
$AuNi/Al_2O_3$	0.1	0	[37]
$PdCu/Al_2O_3$	1	1	[46]

donor stage when an ion-radical of CO_2^- returns the electron to catalyst. The electron transfer may proceed easier when not only reduced metal but also metal oxide forms exist in the catalyst; at the metal-oxide interface the barrier of CO molecule activation should be decreased.[37,43]

Thiophene oxidation by hydrogen peroxide on monometallic and bimetallic NiMo and NiW catalysts

The possibility of LED deposition of uniform bimetallic oxide coatings comprising Ni and Mo or W on alumina support when using a pressed mixture of their powders as a target has been recently demonstrated.[15]

This work compares the structure and properties of such bimetallic LED catalysts with their monometallic counterparts on the example of thiophene oxidation with hydrogen peroxide. The main product of this reaction on both monometallic (Mo and W) and bimetallic catalysts is sulfuric acid. The kinetic curves of thiophene conversion are compared in Figure 5.

The Ni/Al_2O_3 catalysts were totally inactive in this reaction regardless of Ni loading (0.05 or 0.005 wt.%). Ni is known to be significantly less active in thiophene oxidation than metals of V–VI groups.[18] In contrast, both Mo/Al_2O_3 and W/Al_2O_3 showed remarkable activity in thiophene oxidation. However, the Ni-containing bimetallic catalysts demonstrated higher activities than monometallic Mo/Al_2O_3 and W/Al_2O_3. Therefore, inactive Ni greatly improves the catalytic performance of Mo and W. This improvement can be explained by two reasons: (I) nickel species in bimetallic catalysts introduce additional adsorption centres on the catalyst surface, providing strong chemisorption of thiophene;[50] moreover, Ni^0 is more active than NiO;[51] (II) the addition of Ni changes the electronic structure and redox properties of W and Mo species that are responsible for the oxidation of thiophene.

Indeed, according to XPS data, the addition of Ni to the catalysts changes the oxidation state of Mo and W. The percentage of the partly or totally reduced species (W^{4+}, Mo^{4+}, W^0 and Mo^0) increases with the addition of Ni. We earlier showed for Mo, that the co-existence of different electronic states enhances the catalytic efficiency.[52,53] For the catalysts studied in this work the effect is the most prominent for W-containing samples: NiW/Al_2O_3 catalysts demonstrate the highest efficiency in thiophene oxidation (Figure 5). TOF values (Table 5) calculated on the base of initial reaction rates and loadings of active Mo and W metals confirm this conclusion. These values can only be used as an estimation because the number of active centres on the surface is not known, so the metal loadings were used in this calculation instead. Nevertheless, it is certain that calculated TOF values in this case are very high. Orders of magnitude lower values are characteristic for known catalysts of the thiophene oxidation with hydrogen peroxide. Thus, at similar reaction conditions the TOF value estimated from the data[54] for impregnated heterogeneous catalyst on the base of ammonium polytungstate is 25 h^{-1}. The most efficient catalyst on the base of $H_3PW_{12}O_{40}$ and a catalytically active ionic liquid provides TOF value of 140 h^{-1},[55] whereas TOF of LED prepared NiW/Al_2O_3 catalyst reaches 7700 h^{-1} (Table 5). The reason of this high activity may be also related to the interface interaction providing electron transfer between different electronic states of metals in key stages of oxidation[37,43] as it was described above for CO oxidation.

The stability of catalysts in the considered process is very important because the reaction mixture and the thiophene oxidation product – sulfuric acid cause corrosion of the catalyst. Because of this fact the catalysts in this work were tested for five cycles, feeding new batch of reagents in each cycle. The catalytic properties of mono- and bimetallic Mo and W-containing catalysts are compared in Table 5. Thiophene conversion on monometallic catalysts decreased in each consecutive cycle and after 3–4 cycles these catalysts became inactive. In contrast, bimetallic catalysts showed higher stability. The thiophene conversion on $NiMo/Al_2O_3$ slightly decreased with increasing the number of cycles. NiW/Al_2O_3 showed the highest stability: no changes in thiophene conversion were observed after five cycles. The stability of this catalyst was also confirmed by lower destruction of alumina granules of the support in the aggressive reaction medium. It could be connected with the «core-shell» structure of LED catalysts and the presence of various W/Mo states including Me^0 in bimetallic catalysts. Moreover, the metal oxide layers covering metal nanoparticles and the strong interaction of finely dispersed species with the support may prevent their sintering as well as loss of active phase as a result of diffusion of active components.[56]

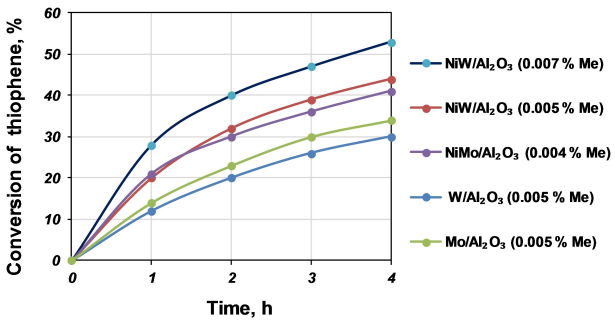

Figure 5. Thiophene conversion vs. reaction time at 60 °C on mono- and bimetallic catalysts comprising Ni, Mo and W.

Table 5. Catalytic properties of mono- and bimetallic alumina supported catalysts comprising Ni, Mo and W. TOF were calculated taking into account only the content of Mo and W active components.

Catalyst	Me [%]	TOF [h^{-1}]	Thiophene conversion [%] in catalytic cycle, 60 °C				
			1	2	3	4	5
$NiMo/Al_2O_3$	0.004	6300	41	34	30	31	29
NiW/Al_2O_3	0.007	7500	53	50	53	51	52
NiW/Al_2O_3	0.005	7700	43	42	43	41	42
Mo/Al_2O_3	0.005	1900	34	30	26	Inactive	Inactive
W/Al_2O_3	0.005	4100	30	27	21	15	Inactive

Unfortunately, the low content of metals (10^{-3} wt.%) limits the physicochemical analysis of the structure of these catalysts and the nature of interface interactions; thus, temperature programmed reduction and XRD methods provide no information. Reliable conclusions about their structure can be made based on TEM, SEM and XPS studies. Due to the "core-shell" structure of LED catalysts, the XPS method turned out to be the most informative. But we can definitely say that the introduction of Ni that is inactive in thiophene oxidation into W or Mo LED catalysts supported on the surface of alumina enhances both the activity and stability of bimetallic catalysts.

Conclusions

This work demonstrated the possibility of the size-selective "dry" technique of laser electrodispersion (LED) for deposition of bimetallic coatings (NiPd, NiMo, NiW) on flat and granulated carbon and oxide supports. For this purpose, both alloy and compacted metal powders can be used as targets for the laser exposure, and the target composition will determine metal ratio on the catalyst surface. The coatings comprise metal nanoparticles several nanometers in size uniformly distributed over the support surface. In accordance with EDS and XPS both metals are located at the same areas on the outer support surface and contact with each other. As a result, new electronic states of metals and metal-oxide interfaces are formed in bimetallic coatings.

The uniform distribution of finely dispersed metal particles, along with the existence of both metallic and oxidized states of metal atoms provides the high concentration and availability of active sites in LED catalysts. However, an accurate estimate of the metal states and interface nature in these low-loaded catalysts is now a rather difficult task. XPS study was found to be the most informative method due to "crust-like" structure of LED systems. The fraction of oxidized and reduced metal forms can be tuned depending on metal loading and the nature of a support (alumina or carbon). The optimal ratio between these forms and the interaction between two metals provide significant improvement of catalytic action in comparison with monometallic counterparts and usual supported catalysts prepared by chemical methods.

Bimetallic LED catalysts with very low metal loading (mainly 0.005 wt.%) demonstrated high activity and stability in environmentally important reactions: carbon monooxide oxidation with O_2 on NiPd and tiophene oxidation with H_2O_2 on NiW(Mo). Due to the presence of reduced metals on the surface of LED catalysts they are very stable in the corrosive reaction medium of oxidative desulfurization.

Thus, LED technique opens new ways for developing of highly active and stable catalysts, not only monometallic, but also bimetallic, with ultra-low metal loading. The proposed LED method is one-stage, well controlled and does not require the use of solutions of chemicals and solvents, which makes it very promising for the design of bimetallic catalysts for different redox reactions.

Experimental Section

Pure metal targets (Ni, Pd, Mo, W) were used for deposition of monometallic particles on a support by LED. The bimetallic NiPd catalysts were synthesized from NiPd (atomic ratio 77:23) alloy target as described in,[14] while compacted mixture of metal powders with the Ni:W(Mo) atomic ratio of 50:50 were used for the preparation of $NiMo/Al_2O_3$ and NiW/Al_2O_3 catalysts. The way of target production from the mixture of two metal powders is described in S2 SM.

Granules of γ-Al_2O_3 (JPS "Katalizator", Russia, $S = 180\ m^2/g$, 0.4–1.0 mm grain size) and Sibunit,[57] material composed of carbon black and pyrolytic graphite (2.5–3.0 mm grain size) were used as supports for catalyst preparation. During LED deposition of metals the granules of a support were placed on a vibrating piezoceramic plate to achieve the uniform distribution of metal particles on the support surface.

To determine the deposition rate of metal nanoparticles which is important to estimate the metal loadings, a smooth flat substrate was used as a support. A quartz thickness sensor was taken for this purpose, and the shift of the resonating frequency from the initial value of 3.3 MHz was measured during deposition. The measured deposited mass vs. time dependences for the samples produced using mono- and bimetallic targets are shown in SM, Figure S12. In all cases the dependences were close to linear. The calculated deposition rates (Table 6) are similar for different metals, for bimetallic powder targets they are slightly higher.

The time (T) required for deposition of N layers of nanoparticles on the external surface of pellets was calculated using the following equation:

$$T = \pi \frac{\rho_P}{\rho_S} \frac{d}{D} \frac{M}{v S_0} N, \quad (1)$$

where ρ_P – density of deposited metal particles, d – diameter of metal particle, ρ_S – density of support pellets, D – diameter of support pellets, M – support mass, v – deposition rate (Table 6), $S_0 = 3.14\ cm^2$ – area of the cuvette densely filled with support granules. This equation takes into account that nanoparticles are deposited only on the external surface of pellets. The metal loading in the catalysts can be calculated using equation:

$$C = \pi \frac{\rho_P}{\rho_S} \frac{d}{D} N. \quad (2)$$

Two model samples with different metal loadings (0.1 and 0.5 NPL) were prepared by LED deposition of metal nanoparticles from Ni, Pd, and NiPd targets on HOPG. Another type of model samples for TEM studies was prepared by the deposition metal nanoparticles from Pd (0.1 and 1.0 NPL) and NiMo targets on the copper TEM grids covered with carbon.

Estimated metal loading in catalysts on granulated Sibunit and Al_2O_3 supports are presented in Table S2, SM.

X-ray photoelectron spectra (XPS) were recorded on an Axis Ultra DLD spectrometer (Kratos analytical, UK) using monochromatic AlKα radiation. The pass energy of the analyser was 160 eV for survey spectra and 40 eV for high resolution scans. The Kratos

Table 6. Deposition rates of nanoparticle coatings on the flat support by LED.

Metal	Ni	Mo	Pd	W	NiPd	NiMo	NiW
Deposition rate, [μg/(cm² min)]	1.9	2.4	3.9	3.0	5.0	7.0	4.0

charge neutralizer was used for alumina supported samples and the spectra were charge-corrected to give Al2p peak a binding energy of 74.7 eV.

The samples were studied by transmission electron microscopy (TEM) on a JEOL JEM 2100F/UHR instrument (Japan) equipped with EDS accessory. Bright field and high-angle annular dark field (HAADF) modes were used.

The catalyst surfaces were examined on a JEOL JSM-6000 NeoScope scanning electron microscope with a built-in EX-230 energy dispersive X-ray analyser. The images were recorded in the secondary electron imaging (SEI) mode in a high vacuum at an accelerating voltage of 5 kV.

Catalysts were tested in CO oxidation using the pulse microcatalytic method in a quartz tubular fixed-bed flow-type reactor. 100 mg of catalyst was placed into the reactor on a Schott filter. Helium at atmospheric pressure was continuously passed through the reactor at a flow rate of 60 ml/min. The stoichiometric reaction mixture (2 vol.% CO, 1 vol.% O_2, 97 vol.% He) was fed into He flow by pulses (10 pulses per hour) using a six-way valve with a 1 mL gas loop.

The concentrations of CO and CO_2 in the reaction mixture were measured by a GC (thermal conductivity detector; packed column PorapakQ) using the EcoChrom software package for data processing. The CO conversion was calculated from the GC peak areas of CO and CO_2 using pre-measured calibration curves. The steady-state CO conversion for each reaction temperature was calculated after 4–20 pulses.

Ni, Mo, and W catalysts were tested as described in.[15] The model mixture (10 ml of 1 wt.% thiophene solution in isooctane, 0.1 g of the catalyst and 0.4 ml of 50% H_2O_2) was placed in a thermostated reactor equipped with a stirrer. The process was carried out at 60 °C and samples of the organic phase were periodically collected for GC-FID analysis on a Kristall 2000M chromatograph (Chromatec, Russia) with a capillary column (Zebron ZB-1, 30 m × 0.32 mm i.d. × 0.5 μm). After a standard 4-hour test, the liquid phase was drained and a new portion of the reagents was fed in the reactor. This cycle was repeated 5 times.

Acknowledgements

This work was supported by the Russian Foundation for Basic Research (project 19-33-90024). The authors acknowledge support from Lomonosov Moscow State University Program of Development for providing access to the XPS and TEM facilities.

Conflict of Interest

The authors declare no conflict of interest.

Keywords: laser electrodispersion · nanoparticles · bimetallic catalysts · heterogeneous catalysis · oxidation · carbon monoxide · thiophene

[1] O. G. Ellert, M. V. Tsodikov, S. A. Nikolaev, V. M. Novotortsev, *Russ. Chem. Rev.* **2014**, *83*, 718–732.
[2] V. Ponec, *Appl. Catal. A* **2001**, *222*, 31–45.
[3] V. Dal Santo, A. Gallo, A. Naldoni, M. Guidotti, R. Psaro, *Catal. Today* **2012**, *197*, 190–205.
[4] F. Cai, L. Yang, S. Shan, D. Mott, B. Chen, J. Luo, C.-J. Zhong, *Catalysts* **2016**, *6*, 96.
[5] G. Sharma, A. Kumar, S. Sharma, M. Naushad, R. Prakash Dwivedi, Z. A. ALOthman, G. T. Mola, *J. King Saud Univ. Sci.* **2019**, *31*, 257–269.
[6] J. Zhang, M. Chaker, D. Ma, *J. Colloid Interface Sci.* **2017**, *489*, 138–149.
[7] S. Hong, H. Lee, J. Yeo, S. H. Ko, *Nano Today* **2016**, *11*, 547–564.
[8] J. Yu, J. Nan, H. Zeng, *Appl. Surf. Sci.* **2017**, *402*, 330–335.
[9] T. N. Rostovshchikova, E. S. Lokteva, E. V. Golubina, K. I. Maslakov, S. A. Gurevich, D. A. Yavsin, V. M. Kozhevin, in *Adv. Nanomater. Catal. Energy*, Elsevier, **2019**, pp. 61–97.
[10] E. V. Golubina, E. S. Lokteva, K. I. Maslakov, T. N. Rostovshchikova, M. I. Shilina, S. A. Gurevich, V. M. Kozhevin, D. A. Yavsin, *Nanotechnologies Russ.* **2017**, *12*, 19–26.
[11] E. S. Lokteva, A. A. Peristyy, N. E. Kavalerskaya, E. V. Golubina, L. V. Yashina, T. N. Rostovshchikova, S. A. Gurevich, V. M. Kozhevin, D. A. Yavsin, V. V. Lunin, *Pure Appl. Chem.* **2012**, *84*, 495–508.
[12] T. N. Rostovshchikova, M. I. Shilina, E. V. Golubina, E. S. Lokteva, I. N. Krotova, S. A. Nikolaev, K. I. Maslakov, D. A. Yavsin, *Russ. Chem. Bull.* **2015**, *64*, 812–818.
[13] T. N. Rostovshchikova, V. V. Smirnov, S. A. Gurevich, V. M. Kozhevin, D. A. Yavsin, S. M. Nevskaya, S. A. Nikolaev, E. S. Lokteva, *Catal. Today* **2005**, *105*, 344–349.
[14] E. V. Golubina, T. N. Rostovshchikova, E. S. Lokteva, K. I. Maslakov, S. A. Nikolaev, T. B. Egorova, S. A. Gurevich, V. M. Kozhevin, D. A. Yavsin, A. Y. Yermakov, *Pure Appl. Chem.* **2018**, *90*, 1685–1701.
[15] A. A. Bryzhin, I. G. Tarkhanova, K. I. Maslakov, S. A. Nikolaev, S. A. Gurevich, V. M. Kozhevin, D. A. Yavsin, M. G. Gantman, T. N. Rostovshchikova, *Russ. J. Phys. Chem. A* **2019**, *93*, 1976–1985.
[16] W. Ahmad, *Sulfur in Petroleum: Desulfurization Techniques*, in T. Saleh (Ed.), *Applying Nanotechnology to the Desulfurization Process in Petroleum Engineering*, Hershey. PA, IGI Global, **2016**, pp. 1–52.
[17] W. N. W. Abdullah, W. A. W. A. Bakar, R. Ali, W. N. A. W. Mokhtar, M. F. Omar, *J. Cleaner Prod.* **2017**, *162*, 1455–1464.
[18] Z. Ismagilov, S. Yashnik, M. Kerzhentsev, V. Parmon, A. Bourane, F. M. Al-Shahrani, A. A. Hajji, O. R. Koseoglu, *Catal. Rev.* **2011**, *53*, 199–255.
[19] V. S. Rudnev, I. V. Lukiyanchuk, M. S. Vasilyeva, V. P. Morozova, V. M. Zelikman, I. G. Tarkhanova, *Appl. Surf. Sci.* **2017**, *422*, 1007–1014.
[20] I. G. Tarkhanova, A. A. Bryzhin, M. G. Gantman, T. P. Yarovaya, I. V. Lukiyanchuk, P. M. Nedozorov, V. S. Rudnev, *Surf. Coat. Technol.* **2019**, *362*, 132–140.
[21] E. B. Gordon, A. V. Karabulin, V. I. Matyushenko, V. D. Sizov, T. N. Rostovshchikova, S. A. Nikolaev, E. S. Lokteva, E. V. Golubina, K. I. Maslakov, I. N. Krotova, et al., *High Energy Chem.* **2016**, *50*, 292–297.
[22] N. E. Kavalerskaya, E. S. Lokteva, T. N. Rostovshchikova, E. V. Golubina, K. I. Maslakov, *Kinet. Catal.* **2013**, *54*, 597–606.
[23] B. K. D. Moulder J. F., Stickle W. F., Sobol P. E., Bomben K. D., *Handbook of X-Ray Photoelectron Spectroscopy*, Perkin-Elmer Corporation Physical Electronics Division 6509 Flying Cloud Drive Eden Prairie, Minnesota 55344 United Stales Of America, **1995**.
[24] T. Pillo, R. Zimmermann, P. Steiner, S. Hüfner, *J. Phys. Condens. Matter* **1997**, *9*, 3987–3999.
[25] A. N. Mansour, *Surf. Sci. Spectra* **1994**, *3*, 231–238.
[26] M. C. Biesinger, B. P. Payne, L. W. M. Lau, A. Gerson, R. S. C. Smart, *Surf. Interface Anal.* **2009**, *41*, 324–332.
[27] L. I. Godina, A. V. Kirilin, A. V. Tokarev, I. L. Simakova, D. Y. Murzin, *Ind. Eng. Chem. Res.* **2018**, *57*, 2050–2067.
[28] R. S. Weatherup, B. C. Bayer, R. Blume, C. Ducati, C. Baehtz, R. Schlögl, S. Hofmann, *Nano Lett.* **2011**, *11*, 4154–4160.
[29] B. C. Bayer, D. A. Bosworth, F. B. Michaelis, R. Blume, G. Habler, R. Abart, R. S. Weatherup, P. R. Kidambi, J. J. Baumberg, A. Knop-Gericke, et al., *J. Phys. Chem. C* **2016**, *120*, 22571–22584.
[30] A. N. Mansour, *Surf. Sci. Spectra* **1994**, *3*, 239–246.
[31] E. V. Golubina, E. S. Lokteva, A. V. Erokhin, A. A. Veligzhanin, Y. V. Zubavichus, V. A. Likholobov, V. V. Lunin, *J. Catal.* **2016**, *344*, 90–99.
[32] D. Teschner, J. Borsodi, A. Wootsch, Z. Revay, M. Havecker, A. Knop-Gericke, S. D. Jackson, R. Schlogl, *Science*, **2008**, *320*, 86–89.
[33] D. Teschner, E. Vass, M. Havecker, S. Zafeiratos, P. Schnorch, H. Sauer, A. Knop-Gericke, R. Schlogl, M. Chamam, A. Wootsch, *J. Catal.* **2006**, *242*, 26–37.
[34] H. Gabasch, K. Hayek, B. Klötzer, W. Unterberger, E. Kleimenov, D. Teschner, S. Zafeiratos, M. Hävecker, A. Knop-Gericke, R. Schlögl, et al., *J. Phys. Chem. C* **2007**, *111*, 7957–7962.

[35] D. O. Scanlon, G. W. Watson, D. J. Payne, G. R. Atkinson, R. G. Egdell, D. S. L. Law, *J. Phys. Chem. C* **2010**, *114*, 4636–4645.
[36] N. Krstajic, V. Jovic, L. Gajickrstajic, B. Jovic, A. Antozzi, G. Martelli, *Int. J. Hydrogen Energy* **2008**, *33*, 3676–3687.
[37] Z.-J. Zhao, Z. Li, Y. Cui, H. Zhu, W. F. Schneider, W. N. Delgass, F. Ribeiro, J. Greeley, *J. Catal.* **2017**, *345*, 157–169.
[38] M. Haneda, M. Todo, Y. Nakamura, M. Hattori, *Catal. Today* **2017**, *281*, 447–453.
[39] M. S. Chen, Y. Cai, Z. Yan, K. K. Gath, S. Axnanda, D. W. Goodman, *Surf. Sci.* **2007**, *601*, 5326–5331.
[40] S. A. Nikolaev, E. V. Golubina, M. I. Shilina, *Appl. Catal. B* **2017**, *208*, 116–127.
[41] S. A. Nikolaev, E. V. Golubina, L. M. Kustov, A. L. Tarasov, O. P. Tkachenko, *Kinet. Catal.* **2014**, *55*, 311–318.
[42] A. K. Gatin, M. V. Grishin, S. A. Gurevich, N. V. Dokhlikova, A. A. Kirsankin, V. M. Kozhevin, E. S. Lokteva, T. N. Rostovshchikova, S. Y. Sarvadii, B. R. Shub, et al., *Russ. Chem. Bull.* **2015**, *64*, 2337–2343.
[43] J. Deng, W. Song, M. Jing, T. Yu, Z. Zhao, C. Xu, J. Liu, *Catal. Today* **2020**, *339*, 210–219.
[44] O. Balmes, A. Resta, D. Wermeille, R. Felici, M. E. Messing, K. Deppert, Z. Liu, M. E. Grass, H. Bluhm, R. van Rijn, et al., *Phys. Chem. Chem. Phys.* **2012**, *14*, 4796.
[45] K.-S. Cho, Y.-K. Lee, *J. Korean Phys. Soc.* **2012**, *61*, 293–296.
[46] M. Gennero de Chialvo, A. Chialvo, *J. Electroanal. Chem.* **1998**, *448*, 87–93.
[47] D. W. Bassett, H. W. Habgood, *J. Phys. Chem.* **1960**, *64*, 769–773.
[48] E. S. Lokteva, T. N. Rostovshchikova, S. A. Kachevskii, E. V. Golubina, V. V. Smirnov, A. Y. Stakheev, N. S. Telegina, S. A. Gurevich, V. M. Kozhevin, D. A. Yavsin, *Kinet. Catal.* **2008**, *49*, 748–755.
[49] N. Turaeva, M. L. Preuss, *Catal. Commun.* **2015**, *65*, 30–33.
[50] W. Malone, H. Yildirim, J. Matos, A. Kara, *J. Phys. Chem. C* **2017**, *121*, 6090–6103.
[51] I. Babich, *Fuel* **2003**, *82*, 607–631.
[52] I. G. Tarkhanova, A. V. Anisimov, A. K. Buryak, A. A. Bryzhin, A. G. Ali-Zade, A. V. Akopyan, V. M. Zelikman, *Pet. Chem.* **2017**, *57*, 859–867.
[53] I. G. Tarkhanova, A. V. Anisimov, S. V. Verzhichinskaya, A. K. Buryak, V. M. Zelikman, M. G. Gantman, *Pet. Chem.* **2016**, *56*, 158–165.
[54] B. Zhang, Z. Jiang, J. Li, Y. Zhang, F. Lin, Y. Liu, C. Li, *J. Catal.* **2012**, *287*, 5–12.
[55] A. A. Bryzhin, M. G. Gantman, A. K. Buryak, I. G. Tarkhanova, *Appl. Catal. B* **2019**, *257*, 117938.
[56] S. Takenaka, R. Kaji, K. Sugiyama, R. Ida, *Appl. Catal. A* **2018**, *566*, 52–59.
[57] Y. I. Yermakov, V. F. Surovikin, G. V. Plaksin, V. A. Semikolenov, V. A. Likholobov, L. V. Chuvilin, S. V. Bogdanov, *React. Kinet. Catal. Lett.* **1987**, *33*, 435–440.

Manuscript received: March 23, 2020
Revised manuscript received: May 23, 2020
Accepted manuscript online: May 25, 2020
Version of record online: ■■, ■■■

FULL PAPERS

Laser electrodispersion: Unusual high catalytic activity in CO and thiophene oxidation was found for low percentage NiPd and NiMo/W catalysts on alumina and carbon supports prepared by laser electrodispersion of targets from alloy or pressed mixture of metal powders.